SCIENCE CHINA Materials ARTICLES

mater.scichina.com link.springer.com

Published online 13 October 2020 | https://doi.org/10.1007/s40843-020-1489-6
Sci China Mater 2020, 63(12): 2551–2559

The effect of air exposure on device performance of flexible C8-BTBT organic thin-film transistors with hygroscopic insulators

Pengshan Xie, Tianjiao Liu, Pei He, Guozhang Dai, Jie Jiang, Jia Sun* and Junliang Yang*

ABSTRACT **Organic thin film transistors (OTFTs) are normally sensitive to ambient conditions and show performance degradation in air. On the contrary, the performance of flexible 2,7-dioctyl[1] benzothieno [3,2-*b*][1]benzothiophene (C8-BTBT) OTFTs using cross-linked polymer layer, poly(4-vinyl-phenol)-4,4'-(hexafluoroisopropylidene) diphthalic anhydride (PVP-HDA), as the dielectric layer can be improved in air conditions with 40% relative humidity. Under soaking in air with 40% relative humidity, the electrical behavior, surface morphology, and contact angle of the flexible C8-BTBT OTFTs using PVP-HAD as dielectric layer with three different thicknesses were investigated. It is found that, when the devices with 375 nm-thick PVP-HDA films are placed in 40% relative humidity air conditions for 6 h, the corrected average mobility (μ) can increase from 3.2 to 5.1 $cm^2 V^{-1} s^{-1}$. Furthermore, the average threshold voltage (V_{th}) changes from −12.4 to −9.3 V while keeping a constant ratio of $I_{on}/I_{off} = 10^4$. These results indicate that the flexible C8-BTBT OTFTs with PVP-HDA dielectric layer exhibit interesting application prospects.**

Keywords: flexible electronics, C8-BTBT, OTFTs, PVP-HDA, hygroscopicity, air stability.

INTRODUCTION

Over the past years, significant developments in organic thin film transistors (OTFTs) have been made, and the mobility (μ) has been increased to over 43 $cm^2 V^{-1} s^{-1}$ [1]. It is well known that OTFTs have the advantages of solution process, flexibility, low cost, large area, and so on [2–5]. Thus, OTFTs show great potential applications in sensors, circuits, and synaptic electronics [6–11], also thanks to the improvement of device performance *via* new active materials, device engineering, interface engineering of dielectric layer, etc. [12–16]. Air stability is one of the most important issues for meeting the requirements in practical applications [17–21]. In previous studies, organic materials affected by air environment have been widely studied [22,23]. It has been reported that for gate dielectric materials with active functional groups, such as hydroxyl groups, the interaction with the adsorbed water in air would affect the device performance [24,25], leading to performance degradation in air [26,27].

As a typical gate dielectric layer material, cross-linked polymer, poly(4-vinyl-phenol)-4,4'-(hexafluoroisopropylidene) diphthalic anhydride (PVP-HDA), can be prepared *via* solution processes and exhibits excellent insulating properties [28]. Furthermore, 2,7-dioctyl[1] benzothieno[3,2-*b*][1]-benzothiophene (C8-BTBT) is one of the most promising high-mobility p-channel semiconductor material in OTFTs [29–31]. Herein, the effect of air exposure with 40% relative humidity on the device performance of flexible C8-BTBT OTFTs with cross-linked polymer PVP-HDA as the dielectric layer was studied in details. The flexible C8-BTBT OTFTs were fabricated using a structure of bottom-gate/top-contact on poly(ethylene terephthalate) (PET) covered with indium tin oxide (ITO) as the gate electrode. The mobility of the device was found to increase initially and then decline upon increasing the exposure time. Since the C8-BTBT has good air stability and the PVP-HDA cross-linked polymer gate dielectric film has the ability to absorb water from air, it is deduced that the performance changes are mainly caused by the PVP-HDA films. By comparing devices consisting of PVP-HDA films with different thicknesses, namely 650, 375, and 280 nm, it can be seen that the humidity influence becomes weaker with

Hunan Key Laboratory for Super-microstructure and Ultrafast Process, School of Physics and Electronics, Central South University, Changsha 410083, China
* Corresponding authors (emails: jiasun@csu.edu.cn (Sun J); junliang.yang@csu.edu.cn (Yang J))

decreasing thickness of PVP-HDA films.

EXPERIMENTAL SECTION

C8-BTBT was purchased from Jilin Optical and Electronic Materials Co., Ltd. and used without purification. PVP, HDA, and triethylamine (TEA) were purchased from Sigma-Aldrich, and were also employed without further purification. OTFTs were fabricated with the conventional structure, consisting of bottom-gate/top-contact. The flexible PET films covered with ITO were selected as substrates. Furthermore, the substrates were ultrasonically cleaned with DI water, acetone, and isopropanol for 5 min each. After cleaning, the films were dried with nitrogen gas. PVP (1 g) and 100 mg of HDA were dissolved in 5 mL of propylene glycol monomethyl ether acetate (PGMEA), separately. In order to achieve a better dissolution, the two solutions were stirred overnight. Afterwards, 10 μL of TEA was added into the PVP solution in PGMEA and mixed thoroughly. PVP and HDA solutions were then mixed and stirred for 2 h to obtain a full cross-link between the two materials. Finally, the solution was filtered through a 0.45-μm syringe filter. Central spin coating (CSC) was used to fabricate the gate dielectric layer. During the CSC deposition, spin-coating speeds of 1000, 3000, and 6000 rpm were adopted to fabricate films with different thicknesses. The PVP-HDA films were placed on the hotplate at 100°C for 1 h to promote the cross-linking reaction after spin coating. During the off-center spin coating (OCSC) process, C8-BTBT was dissolved in chlorobenzene (CB) with a concentration of 5 mg mL^{-1}. Polystyrene (PS) was added into the C8-BTBT solution as an additive (10 wt% of PS) [1,32]. The C8-BTBT:PS semiconductor layer was fabricated onto different PVP-HDA films *via* the same OCSC process in the N_2-golve box. Finally, 50-nm-thick Au source and drain electrodes were deposited at a pressure of ~8×10^{-4} Pa on C8-BTBT films with a shadow mask, resulting in a channel width and length of 1000 and 80 μm, respectively.

The morphologies of the PVP-HDA thin films with different air exposure times and different thicknesses were examined by atomic force microscope (AFM, Agilent Technologies 5500AFM/SPM System). The change of dielectric layer capacitance was measured *via* an impedance tester (IM3536, HIOKI, Japan). Scanning electron microscope (SEM, FEI Helios Nanolab 600i, USA) was also used to identify the change of oxygen content and display the cross-section morphology of the devices. All OTFTs were measured with a Keithley 4200 SCS semiconductor parameter analyzer under ambient conditions with a relative humidity of 40%. The field-effect mobility was extracted from the saturated region of the transfer characteristics according to Equation (1):

$$\mu = \frac{2L}{W} \times \frac{I_D}{C_i \times (V_G - V_{th})^2}, \quad (1)$$

where μ the is the field-effect mobility, W/L represents the ratio of channel width/length, C_i is the capacitance per unit area, V_G is the gate voltage, and V_{th} represents the threshold voltage.

RESULTS AND DISCUSSION

In order to explore the effects of different exposure times in air with 40% relative humidity on the device performance, the devices with 375 nm-thick gate dielectric layers were fabricated. The structure of the device is shown in Fig. 1a. The statistical data of V_{th} and μ are shown in Fig. 1b, c. The average μ of these devices increases from 8.1 to 11.5 $cm^2 V^{-1} s^{-1}$ in the first 6 h, and then decreases to 10.4 and 8.7 $cm^2 V^{-1} s^{-1}$ in 12 and 18 h, respectively. Correspondingly, the average value of V_{th} decreases from −12.3 to −7.2 V. The V_{th} drops significantly in the first 12 h and then gradually saturates within the following 6 h. The photograph of the C8-BTBT flexible OTFT (f-OTFT) array is shown in Fig. 1d. The transfer characteristic curves of the devices with Si/SiO_2 as the substrate and gate electrode are shown in Fig. S1a, and the structure diagram is shown in Fig. S1b. The red curve represents the initial device, while the black curve represents the device after being placed in 40% humidity air conditions for 18 h. By comparing the two states, it can be seen that there is no big difference in the performance. Therefore, short-term and low-humidity exposure have little effect on the C8-BTBT layer.

At present, there are still several issues concerning the mobility calculation of f-OTFTs. A large number of studies have demonstrated that the OTFT mobility is overestimated when using the traditional transistor theory, since the equations used to calculate the mobility are valid only for ideal OTFTs. Very recently, Choi *et al.* [33] described several types of error calculations in detail and proposed a parameter, the measurement reliability factor *r*, to quickly gauge the overall effectiveness of mobility.

In order to obtain a more reliable μ value, the factor *r* was also introduced in the present work, and it is given by:

$$r = \left(\frac{\sqrt{|I_{ds}|^{max}} - \sqrt{|I_{ds}^0|}}{|V_G|^{max}} \right)^2 \div \left(\frac{WC_i}{2L} \times \mu \right)_{initial}, \quad (2)$$

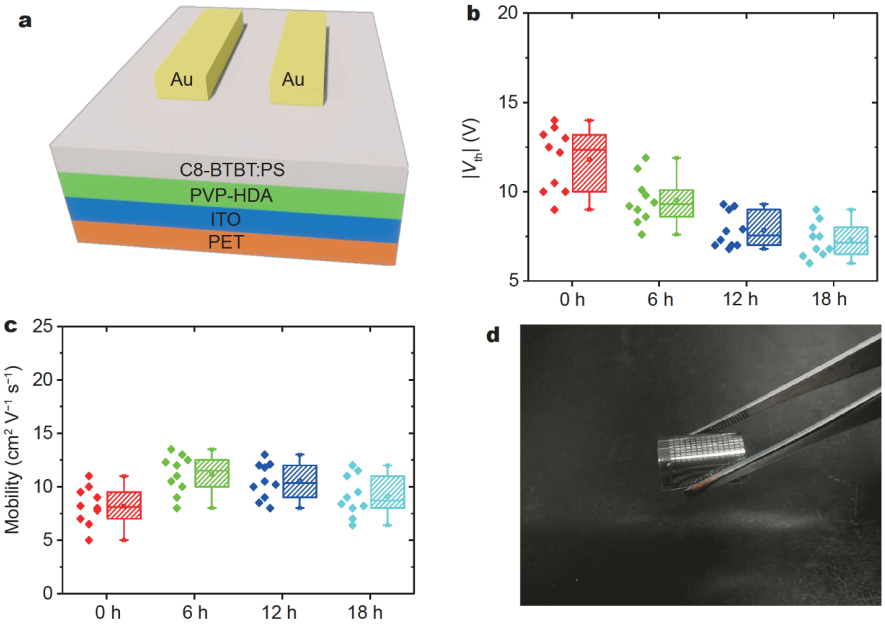

Figure 1 (a) Schematic diagram of the OTFTs with a bottom-gate/top-contact structure. (b) Statistical V_{th} and (c) μ of the devices with a 375-nm-thick PVP-HDA film. (d) Photograph of the flexible C8-BTBT OTFTs array.

where $|I_{ds}|^{max}$ is the experimental maximum source–drain current at the maximum gate voltage $|V_G|^{max}$. According to this method, the mobility of the devices was re-calculated as: $\mu_{initial} \times r$. The transfer characteristic curves of our devices can be considered similar to the one of the overestimated cases described in [33]. Table 1 shows the factor r and corrected μ of the devices with 375-nm-thick gate dielectric layers.

Table 1 The reliable factor r and corrected μ of the devices with 375-nm-thick gate dielectric layers

Time (h)	0	6	12	18
r	0.40	0.44	0.45	0.52
$\mu_{initial}$ ($cm^2 V^{-1} s^{-1}$)	8.1	11.5	10.4	8.7
$\mu_{corrected}$ ($cm^2 V^{-1} s^{-1}$)	3.2	5.1	4.7	4.5

The typical transfer characteristic curves for the devices with four different exposure times are shown in Fig. 2. The V_{th} starts to decrease from −9.5 V and finally saturates at about −5 V (shown in Fig. 2a–d). The I_{ds} also increases with the exposure time prolonging. However, as the exposure time increases, the I_{on}/I_{off} ratio has a significant reduction, as shown in Fig. 2c, d. The device exposed for 18 h shows a decreased I_{on}/I_{off} ratio of 10^2. This means that the gate dielectric and the interface between PVP-HDA and C8-BTBT are most subjected to degradation. Furthermore, the hysteresis phenomenon gradually disappears with increasing exposure time, but not in an ordinary way. It is clear that the reduction of the hysteresis window is mainly caused by the obvious reduction of $|V_{th}|$, even if the intersection of the reverse sweep extension line and the X-axis would increase with longer exposure time. The voltage at the intersection increases from −4 to −7.8 V. Therefore, the performance of OTFT devices could degrade with exposure to a wet environment, different from the results of many previous reports. The C8-BTBT is a p-type material and has high water-oxygen resistance and air stability [34].

As discussed above, it is speculated that the changes of the performance are related to the PVP-HDA films. It is believed that the PVP-HDA layer could absorb water in air, thus having obvious effects on the performance of the device. In order to further explore the effect of air exposure on PVP-HDA films, the flexible C8-BTBT OTFTs were fabricated with three different thicknesses of dielectric layer.

The characterization of the film thickness was achieved by using a step profiler. Upon increasing the rotation speed, the PVP-HDA films become thinner. The 650, 375, and 280 nm thicknesses correspond to films fabricated *via* 1000, 3000, and 6000 rpm, respectively. In order to calculate the μ more accurately, the variation of C_i with thickness and exposure time is shown in Table 2. The specific capacitance extracted from 20 Hz was used to calculate μ. The C_i would increase with increasing exposure time regardless of the thickness. This also shows

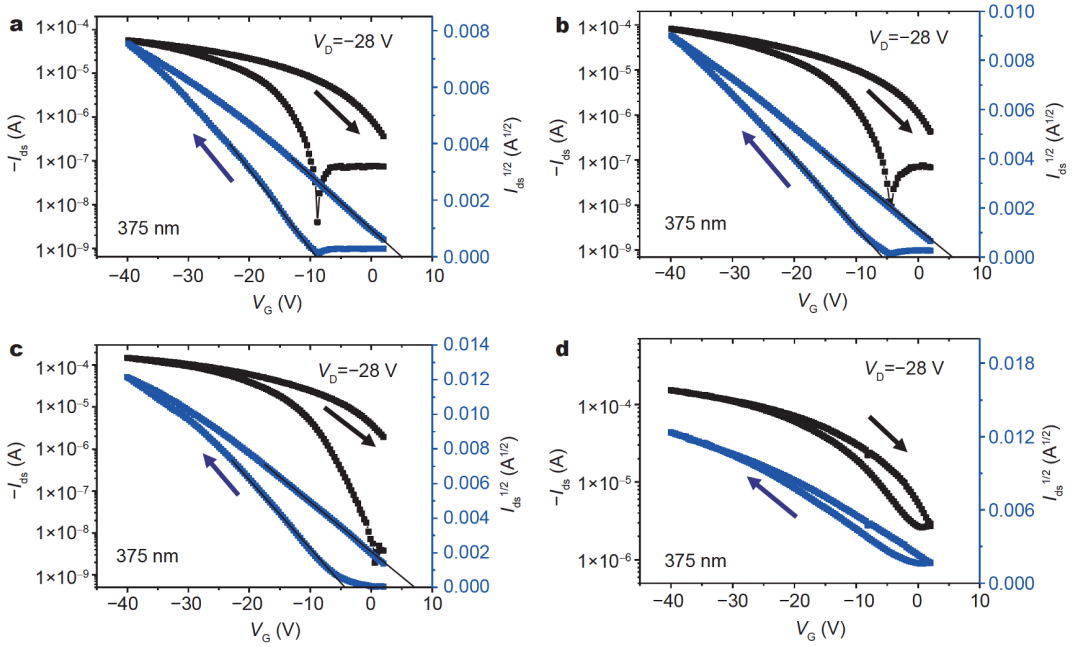

Figure 2 Typical characteristic curves of the device with a 375-nm-thick PVP-HDA film. The device was placed in 40% humidity air conditions for (a) 0 h, (b) 6 h, (c) 12 h, and (d) 18 h.

the tendency for the thicker PVP-HDA film to undergo greater changes with increasing exposure time. The changes become more obvious in the first 12 h. The line graphs are shown in Fig. S2.

Table 2 not only compares the changes of C_i which are related to the thickness of PVP-HDA films, but also illustrates that wet environment can increase the C_i, which is supposed to cause a decrease in μ. In order to further explore the influence of humidity, the devices fabricated with three different thicknesses of PVP-HDA films were placed in air ambient with 40% relative humidity for 6 h, and then compared with the initial devices. The transfer characteristic curves are shown in Fig. 3.

Fig. 3a–c show the devices with three different thicknesses of PVP-HDA films, while a clear difference in V_{th} and μ can be observed in Fig. 3d–f. Regardless of the thickness, the μ and V_{th} of the devices change significantly after being explored in 40% humidity air conditions for 6 h. Furthermore, the saturation currents of the devices rise noticeably for 650 and 375-nm-thick PVP-HDA films. The statistical data of V_{th} for the three different devices are shown in Fig. 3d–f. The average V_{th} for the 650-nm-thick PVP-HDA film changes from −17.5 to −11.8 V. In the same situation, the average V_{th} of the devices with 375 and 280-nm-thick PVP-HDA films change from −12.4 to −9.3 V and −5.8 to −4.6 V, respectively. Fig. 3g–i show the statistical data of μ for the three different devices. The devices with 375-nm-thick PVP-HDA have the highest average μ, and the μ value changes from 8.1 to 11.5 $cm^2 V^{-1} s^{-1}$ (Fig. 3h). As shown in Fig. 3g, i, the average μ of the devices with 650 and 280-nm-thick PVP-HDA films change from 0.5 to 0.8 $cm^2 V^{-1} s^{-1}$ and 2.8 to 3.9 $cm^2 V^{-1} s^{-1}$, respectively. Furthermore, the original data for the three different PVP-HDA films were compared with the subtractive values, which were obtained *via* exposing the devices at 40% humidity air conditions for 6 h (shown in Fig. S3). Figs 2, 3 illustrate that the large improvement in saturation current results in a significant increase in μ, especially in the first 6 h.

In order to obtain more reliable changes of μ, the factor r was also introduced, as shown in Table S1. The corre-

Table 2 Change of capacitance of the PVP-HDA films with different thicknesses and exposure times

Time (h)	C_i (10^{-8} F cm^{-2})		
	650 nm	375 nm	280 nm
0	0.72	1.01	1.25
6	0.81	1.10	1.31
12	0.89	1.17	1.33
18	0.91	1.22	1.32
24	0. 94	1.24	1.33

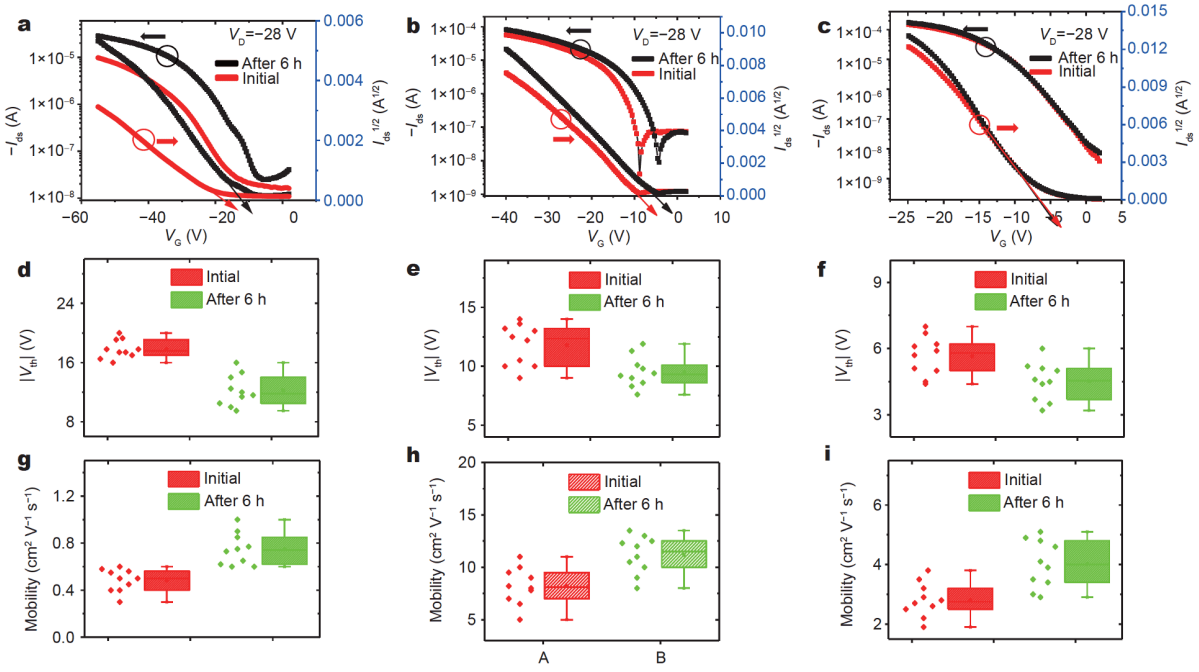

Figure 3 Typical characteristic curves of three different OTFTs and statistical data. The transfer characteristics of the OTFTs with (a) 650, (b) 375, and (c) 280-nm-thick PVP-HDA films as the gate dielectrics, respectively. The red curves represent the initial devices, while the black curves represent the devices after being placed in 40% humidity air conditions for 6 h. (d–f) Statistical data of V_{th} and (g–i) statistical data of μ for 650, 375, and 280-nm-thick PVP-HDA films, respectively.

sponding average μ value is shown in Table S2. Österbacka *et al.* [35,36] demonstrated that PVP is a hygroscopic material and it can absorb water to cause ionic species motion. The ionic motion in the dielectric layer can increase the charge density at the interface between C8-BTBT and PVP-HDA layers, which can increase the saturation current. Another study has considered that PVP as a hydroxyl-rich material could absorb water and cause surface polarization, which also induces a higher saturation current [24]. In addition, hydroxyl groups in the dielectrics have been found to intensively trap electrons and completely eliminate electron transport in a variety of structurally disordered organic semiconductors [37], which may be beneficial to increasing the saturation current.

It is widely known that C_i is linked to both thickness and dielectric constant (ε). The increase of C_i is basically caused by the change of ε, under the assumption that other parameters are unchanged. Thus, the PVP-HDA film absorbs the water, which causes the change of the dielectric constant, and C_i consequently increases. Previous study reported that [38]:

$$V_{th} = \frac{\pm qn_0 d}{C_i} + V_{fb}. \quad (3)$$

Here, q represents the elementary charge, n_0 represents the charge density, d is the film thickness, C_i is the dielectric layer unit area capacitance, and V_{fb} is the flat band voltage, which accounts for any work-function difference between the semiconductor and the gate metal. On one hand, it has been proved that the devices using high-k dielectric materials tend to show a lower $|V_{th}|$ [39]. For PVP-HDA films, whether the rise of C_i is caused by thickness or humidity exposure, it would cause a decline in $|V_{th}|$. The larger capacitance the films have, the smaller V_{th} the devices perform. On the other hand, the AFM surface morphology images of the gate dielectric films with different thicknesses are shown in Fig. 4.

The root mean square (RMS) for all films increases after 12 h exposure in 40% humidity air. A rougher surface of the PVP-HDA layers would trap more free charges. The AFM height images of the C8-BTBT:PS films fabricated on 375-nm-thick PVP-HDA films are also shown in Fig. S4. There is a slight change in the RMS after 12 h exposure in 40% humidity air. This result demonstrates that the C8-BTBT:PS film is relatively stable in these conditions. Pernstich *et al.* [40] demonstrated that, with increasing negative gate voltage, more trap states were filled. In addition, the following equation can be

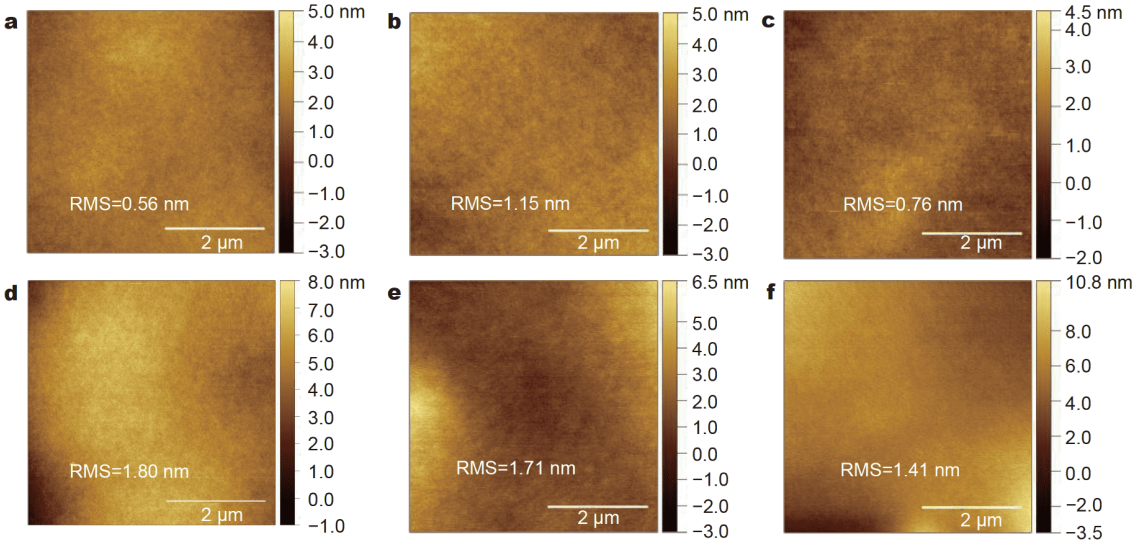

Figure 4 AFM height images of the PVP-HDA films with different thicknesses of (a) 650 nm, (b) 375 nm, and (c) 280 nm. The corresponding images after 12 h exposure for the PVP-HDA films with the thicknesses of (d) 650 nm, (e) 375 nm, and (f) 280 nm.

used to calculate N_{trap}:

$$N_{trap} = C_i \left| V_{tto} \right| / e, \quad (4)$$

where $V_{tto} = V_{th} - V_{to}$, V_{th} means the threshold voltage, and V_{to} represents the turn-on voltage, which is the gate voltage where the drain current starts to increase exponentially. It is possible to obtain N_{trap} from Fig. 2a with $V_{th} = -9.5$ V and $V_{to} = -8.5$ V, as well as from Fig. 2b with $V_{th} = -5.6$ V and $V_{to} = -4.8$ V. Therefore, the N_{trap} values for Fig. 2a, b are 6.32×10^{10} cm^{-2} and 5.50×10^{10} cm^{-2}, respectively.

In order to find out whether water molecules are absorbed by PVP-HDA, elemental analysis in cross-sectional images is shown in Fig. 5. Since a better cross-section could be obtained with a rigid substrate, the devices were fabricated on glass substrates with 375-nm -thick dielectric layer. Then the devices were exposed in 40% humidity air for 12 h and compared with the original films. The cross-sectional images of the two devices can be clearly seen (Fig. 5a, b) and the change of the oxygen element is noticeable. The percentage of the oxygen element changes from 19.8% to 26.1%, which strongly proves that the PVP-HDA dielectric layer absorbs some substances containing oxygen, as shown in Fig. 5c. Furthermore, the devices were tested after 40% humidity exposure for 6 h and stored in the glove box (where the water content is less than 0.1 ppm) for 24 h. It is clear that the performance of the devices would drop, as shown in Fig. S5. The green curves indicate that, after 24 h drying, V_{th} and I_{ds} are close to the initial values. The statistics of V_{th} and saturated I_{ds} are also shown in Fig. S5. In addition, C_i as an important parameter was also tested with the same method, and the statistic values are shown in Fig. S6. It is obvious that the performance of the devices

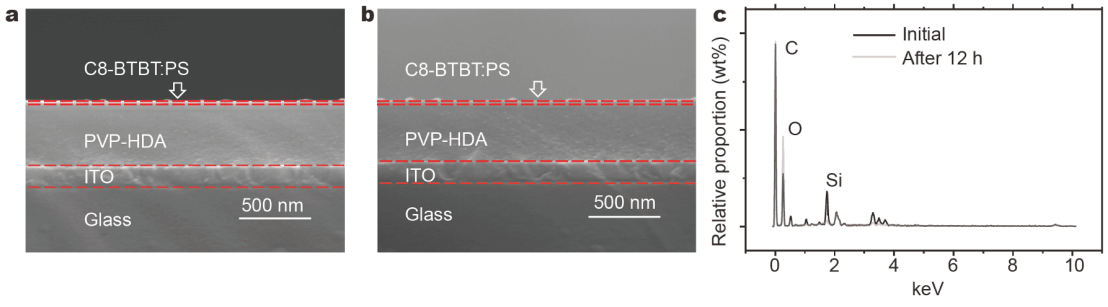

Figure 5 Section diagram of the devices fabricated with 375-nm-thick PVP-HDA film (a) initial and (b) after exposure in 40% humidity air conditions for 12 h. (c) Element content of the two different devices in (a) and (b).

would recover after drying, including V_{th}, saturated I_{ds}, and C_i. The phenomenon illustrates that the changes of the devices can be eliminated after a period of drying and further proves the presence of absorbed water in the PVP-HDA films.

The PVP-HDA films with three different thicknesses were exposed in air environment with humidity of 40% for 12 h and the evolution of the contact angles was compared, as shown in Fig. S7. The contact angle has an observable change, regardless of the thickness of the films. The change of contact angle of the PVP-HDA films with different thicknesses is slightly different. However, the film with a thickness of 650 nm has the most obvious change from 70.1° to 68.1° (Fig. S7a, b). The other films have slightly different contact angle, which is shown in Fig. S7c–f. The decrease of contact angle means the hydrophilicity of the films has been improved [41].

This also proves that the PVP-HDA films could be affected by wet environment and could absorb water from air. In Pernstich's study, it was demonstrated that a self-assembled monolayer (SAM) with a permanent electric dipole field inserted between the gate insulator and the pentacene would increase the band bending and enhance hole density in the channel [40]. Jung *et al.* [24] also demonstrated that, when the dielectric is porous, water molecules could be absorbed in the dielectric layer causing a greater amount of polarization in the dielectric. This effect can vastly overwhelm the bias stress and cause an increase in the drain current. It is believed that the parameters of the devices (including V_{th}, I_{ds}, and μ) are changed due to both the adsorbed water and PVP-HDA films. On one hand, for the PVP-HDA films with same thickness, the rise of C_i with increasing exposure time would lead to a high carrier density and the decrease of the absolute value of V_{th} [42]. On the other hand, even weak dopants can improve the device performance [43]. It is considered that the protons diffuse into the hygroscopic dielectric layer, resulting in doping of the semiconducting channel and increase of I_{ds} [44–46].

CONCLUSIONS

In conclusion, flexible C8-BTBT OTFT devices were fabricated with three different thicknesses of PVP-HDA films. It was proven that short-term air exposure for 6 h could improve the performance of the devices, including μ (the corrected average value changes from 3.2 to 5.1 $cm^2 V^{-1} s^{-1}$) and V_{th} (the average value changes from −12.4 to −9.3 V). However, with the exposure time increasing beyond 6 h, the insulation property and surface morphology of the PVP-HDA films were found to suffer some degradation and had a negative effect on I_{on}/I_{off} and μ. Furthermore, the thicker PVP-HDA film has a more significant impact on the device performance, which is possibly due to the stronger water absorption. As demonstrated above, different from previous studies where the wet environment was shown to degrade the performance of OTFTs, in the present study our devices showed an enhanced electrical performances under a short-term air exposure. Therefore, it is envisaged that these results will provide a guiding role for the fabrication of high-performance OTFT devices in air environment.

Received 27 February 2020; accepted 11 August 2020; published online 13 October 2020

1 Yuan Y, Giri G, Ayzner AL, *et al.* Ultra-high mobility transparent organic thin film transistors grown by an off-centre spin-coating method. Nat Commun, 2014, 5: 3005
2 Giri G, Verploegen E, Mannsfeld SCB, *et al.* Tuning charge transport in solution-sheared organic semiconductors using lattice strain. Nature, 2011, 480: 504–508
3 Duan S, Gao X, Wang Y, *et al.* Scalable fabrication of highly crystalline organic semiconductor thin film by channel-restricted screen printing toward the low-cost fabrication of high-performance transistor arrays. Adv Mater, 2019, 31: 1807975
4 Yang J, Yan D, Jones TS. Molecular template growth and its applications in organic electronics and optoelectronics. Chem Rev, 2015, 115: 5570–5603
5 Diao Y, Shaw L, Bao Z, *et al.* Morphology control strategies for solution-processed organic semiconductor thin films. Energy Environ Sci, 2014, 7: 2145–2159
6 Chen Y, Au J, Kazlas P, *et al.* Flexible active-matrix electronic ink display. Nature, 2003, 423: 136
7 Jiang C, Choi HW, Cheng X, *et al.* Printed subthreshold organic transistors operating at high gain and ultralow power. Science, 2019, 363: 719–723
8 Wang S, Xu J, Wang W, *et al.* Skin electronics from scalable fabrication of an intrinsically stretchable transistor array. Nature, 2018, 555: 83–88
9 Tong S, Sun J, Wang C, *et al.* High-performance broadband perovskite photodetectors based on $CH_3NH_3PbI_3$/C8BTBT heterojunction. Adv Electron Mater, 2017, 3: 1700058
10 Qian C, Kong L, Yang J, *et al.* Multi-gate organic neuron transistors for spatiotemporal information processing. Appl Phys Lett, 2017, 110: 083302
11 Kong L, Sun J, Qian C, *et al.* Long-term synaptic plasticity simulated in ionic liquid/polymer hybrid electrolyte gated organic transistors. Org Electron, 2017, 47: 126–132
12 Wei P, Li S, Li D, *et al.* Organic-semiconductor: Polymer-electret blends for high-performance transistors. Nano Res, 2018, 11: 5835–5848
13 Teixeira da Rocha C, Haase K, Zheng Y, *et al.* Solution coating of small molecule/polymer blends enabling ultralow voltage and high-mobility organic transistors. Adv Electron Mater, 2018, 4: 1800141
14 Zhou B, Zhou J, Chen Y, *et al.* Performance improvement of organic phototransistors by using polystyrene microspheres. Sci China Mater, 2018, 61: 737–744

15 Gu PY, Wang Z, Liu G, *et al.* Synthesis, full characterization, and field effect transistor behavior of a stable pyrene-fused *N*-heteroacene with twelve linearly annulated six-membered rings. Chem Mater, 2017, 29: 4172–4175
16 Wu X, Du R, Fang L, *et al.* Grain size adjustion in organic field-effect transistors for chemical sensing performance improvement. Sci China Mater, 2019, 62: 138–145
17 Qian C, Sun J, Zhang L, *et al.* Air-stable and high-performance organic field-effect transistors based on ordered, large-domain phthalocyanine copper thin film. Synth Met, 2015, 210: 336–341
18 Guo X, Ortiz RP, Zheng Y, *et al.* Thieno[3,4-*c*]pyrrole-4,6-dione-based polymer semiconductors: toward high-performance, air-stable organic thin-film transistors. J Am Chem Soc, 2011, 133: 13685–13697
19 Lee WY, Oh JH, Suraru SL, *et al.* High-mobility air-stable solution-shear-processed n-channel organic transistors based on core-chlorinated naphthalene diimides. Adv Funct Mater, 2011, 21: 4173–4181
20 Kim SH, Yang H, Yang SY, *et al.* Effect of water in ambient air on hysteresis in pentacene field-effect transistors containing gate dielectrics coated with polymers with different functional groups. Org Electron, 2008, 9: 673–677
21 Zhang J, Jin J, Xu H, *et al.* Recent progress on organic donor–acceptor complexes as active elements in organic field-effect transistors. J Mater Chem C, 2018, 6: 3485–3498
22 Liu D, Chu Y, Wu X, *et al.* Side-chain effect of organic semiconductors in OFET-based chemical sensors. Sci China Mater, 2017, 60: 977–984
23 Mai J, Tang N, He W, *et al.* Effects of ambient gases on the electrical performance of solution-processed C8-BTBT thin-film transistors. Nanoscale Res Lett, 2019, 14: 169
24 Jung T, Dodabalapur A, Wenz R, *et al.* Moisture induced surface polarization in a poly(4-vinyl phenol) dielectric in an organic thin-film transistor. Appl Phys Lett, 2005, 87: 182109
25 Un HI, Cheng P, Lei T, *et al.* Charge-trapping-induced non-ideal behaviors in organic field-effect transistors. Adv Mater, 2018, 30: 1800017
26 Jurchescu OD, Baas J, Palstra TTM. Electronic transport properties of pentacene single crystals upon exposure to air. Appl Phys Lett, 2005, 87: 052102
27 Goldmann C, Gundlach DJ, Batlogg B. Evidence of water-related discrete trap state formation in pentacene single-crystal field-effect transistors. Appl Phys Lett, 2006, 88: 063501
28 Roberts ME, Queralto N, Mannsfeld SCB, *et al.* Cross-linked polymer gate dielectric films for low-voltage organic transistors. Chem Mater, 2009, 21: 2292–2299
29 Janneck R, Pilet N, Bommanaboyena SP, *et al.* Highly crystalline C8-BTBT thin-film transistors by lateral homo-epitaxial growth on printed templates. Adv Mater, 2017, 29: 1703864
30 Huang Y, Sun J, Zhang J, *et al.* Controllable thin-film morphology and structure for 2,7-dioctyl[1]benzothieno[3,2-*b*][1]benzothiophene (C8BTBT) based organic field-effect transistors. Org Electron, 2016, 36: 73–81
31 Xie P, Liu T, Sun J, *et al.* Solution-processed ultra-flexible C8-BTBT organic thin-film transistors with the corrected mobility over 18 $cm^2/(V\ s)$. Sci Bull, 2020, 65: 791–795
32 Haase K, Teixeira da Rocha C, Hauenstein C, *et al.* High-mobility, solution-processed organic field-effect transistors from C8-BTBT: polystyrene blends. Adv Electron Mater, 2018, 4: 1800076
33 Choi HH, Cho K, Frisbie CD, *et al.* Critical assessment of charge mobility extraction in FETs. Nat Mater, 2018, 17: 2–7
34 He D, Wang Y, Huang Y, *et al.* High-performance black phosphorus field-effect transistors with long-term air stability. Nano Lett, 2019, 19: 331–337
35 Bäcklund TG, Sandberg HGO, Österbacka R, *et al.* Current modulation of a hygroscopic insulator organic field-effect transistor. Appl Phys Lett, 2004, 85: 3887–3889
36 Sandberg H , Bäcklund T , Österbacka R, *et al.* High-performance all-polymer transistor utilizing a hygroscopic insulator. Adv Mater, 2004, 16: 1112–1115
37 Jiang H, Huang Z, Xue G, *et al.* Electron transport at the interface of organic semiconductors and hydroxyl-containing dielectrics. J Mater Chem C, 2018, 6: 12001–12005
38 Egginger M, Bauer S, Schwödiauer R, *et al.* Current *versus* gate voltage hysteresis in organic field effect transistors. Monatsh Chem, 2009, 140: 735–750
39 Sun X, Di C, Liu Y. Engineering of the dielectric–semiconductor interface in organic field-effect transistors. J Mater Chem, 2010, 20: 2599–2611
40 Pernstich KP, Haas S, Oberhoff D, *et al.* Threshold voltage shift in organic field effect transistors by dipole monolayers on the gate insulator. J Appl Phys, 2004, 96: 6431–6438
41 Wei W, Yang C, Mai J, *et al.* High mobility solution-processed C_8-BTBT organic thin-film transistors *via* UV-ozone interface modification. J Mater Chem C, 2017, 5: 10652–10659
42 Fujimoto T, Matsushita MM, Awaga K. Ionic-liquid component dependence of carrier injection and mobility for electric-double-layer organic thin-film transistors. J Phys Chem C, 2012, 116: 5240–5245
43 Wang Z, Zou Y, Chen W, *et al.* The role of weak molecular dopants in enhancing the performance of solution-processed organic field-effect transistors. Adv Electron Mater, 2019, 5: 1800547
44 Yambem SD, Burns S, Arthur JN, *et al.* A highly porous and conductive composite gate electrode for OTFT sensors. RSC Adv, 2019, 9: 7278–7284
45 Elkington D, Belcher WJ, Dastoor PC, *et al.* Detection of saliva-range glucose concentrations using organic thin-film transistors. Appl Phys Lett, 2014, 105: 043303
46 Elkington D, Wasson M, Belcher W, *et al.* Printable organic thin film transistors for glucose detection incorporating inkjet-printing of the enzyme recognition element. Appl Phys Lett, 2015, 106: 263301

Acknowledgements This work was supported by the National Key Research and Development Program of China (2017YFA0206600) and the National Natural Science Foundation of China (51673214).

Author contributions Xie P and Liu T performed the experiments. Xie P, Liu T, Sun J and Yang J prepared the manuscript. Xie P, Sun J, He P, Dai G, Jiang J and Yang J participated in the discussion on experimental results. Yang J directed this project.

Conflict of interest The authors declare no conflict of interest.

Supplementary information Supporting data are available in the online version of the paper.

Pengshan Xie received his BSc degree from the Central South University in 2017. Currently, he is a graduate student at the Central South University. His research interests are focused on the functional layers of high-performance organic thin-film transistors.

Tianjiao Liu received her BSc degree from Hunan Normal University in 2016. She received her MSc degree from the Central South University in 2019. Her research interest focuses on high-performance organic thin-film transistors.

Jia Sun received his PhD degree from Hunan University in 2012. He was a postdoctoral researcher in the Central South University (2012–2014) and Sungkyunkwan University (2017–2018). In 2014, he joined the faculty of Central South University. Now he is a professor in the School of Physics and Electronics. His research interests focus on novel photoelectronic devices and neuromorphic devices.

Junliang Yang received his PhD degree in 2008 from Changchun Institute of Applied Chemistry Chinese (CIAC), Chinese Academy of Sciences (CAS). He then joined Prof. Tim S. Jones's group at the University of Warwick. In April 2011, he moved to the University of Melbourne and the Commonwealth Scientific and Industrial Research Organisation (CSIRO). In 2012, he was appointed as a professor of the School of Physics and Electronics, Central South University. His research focuses on flexible and printed electronics, organic and perovskite solar cells.

空气暴露对基于吸湿绝缘层的C8-BTBT有机薄膜晶体管器件性能的影响

谢朋杉, 刘天娇, 何培, 代国章, 蒋杰, 孙佳*, 阳军亮*

摘要 有机薄膜晶体管(OTFTs)通常对环境条件敏感，在空气中暴露时其性能往往会出现退化. 本文分析了基于聚(4-乙基苯酚)-4,4'-(六氟异丙烯)二酞酸酐交联物绝缘层(PVP-HDA)的2,7-二辛基[1]苯并噻吩[3,2-*b*][1]苯并噻吩(C8-BTBT)柔性OTFTs在40%相对湿度的空气环境中暴露不同时间对器件性能的影响. 研究发现, PVP-HDA绝缘层材料在短时间40%相对湿度的空气下吸附空气中的水分后, 器件的性能有所提升. 其中, 基于375 nm PVP-HAD绝缘层薄膜的柔性OTFTs在相对湿度为40%的空气中放置6小时后，校正后的平均迁移率(μ)由3.2 $cm^2 V^{-1} s^{-1}$提高到5.1 $cm^2 V^{-1} s^{-1}$，平均阈值电压(V_{th})由−12.4 V降低到−9.3 V，开关比仍保持在10^4. 结果表明, 此类OTFT器件有望能够在空气环境中进行大面积制备，并展现出良好的应用前景.

